

---

# Constrained Prompt Enhancement for Improving Zero-Shot Generalization of Vision-Language Models

---

**Xiaojie Yin**  
 Tianjin University  
 xjyin@tju.edu.cn

**Qilong Wang\***  
 Tianjin University  
 qlwang@tju.edu.cn

**Qinghua Hu**  
 Tianjin University  
 huqinghua@tju.edu.cn

## Abstract

Vision-language models (VLMs) pre-trained on web-scale data exhibit promising zero-shot generalization but often suffer from semantic misalignment due to domain gaps between pre-training and downstream tasks. Existing approaches primarily focus on text prompting with class-specific descriptions and visual-text adaptation via aligning cropped image regions with textual descriptions. However, they still face the issues of incomplete textual prompts and noisy visual prompts. In this paper, we propose a novel constrained prompt enhancement (CPE) method to improve visual-textual alignment by constructing comprehensive textual prompts and compact visual prompts from the semantic perspective. Specifically, our approach consists of two key components: Topology-Guided Synonymous Semantic Generation (TGSSG) and Category-Agnostic Discriminative Region Selection (CADRS). Textually, to address the issue of incomplete semantic expression in textual prompts, our TGSSG first generates synonymous semantic set for each category via large language models, and constructs comprehensive textual prompts based on semantic ambiguity entropy and persistent homology analysis. Visually, to mitigate the irrelevant visual noise introduced by random cropping, our CADRS identifies discriminative regions with activation maps outputted by a pre-trained vision model, effectively filtering out noisy regions and generating compact visual prompts. Given the comprehensive set of textual prompts and compact set of visual prompts, we introduce two set-to-set matching strategies based on test-time adaptation (TTA) and optimal transport (OT) to achieve effective visual-textual alignment, and so improve zero-shot generalization of VLMs. Extensive experiments on 10 zero-shot image classification benchmarks, 5 zero-shot out-of-distribution tasks, and 3 zero-shot video action recognition datasets demonstrate that our CPE method clearly outperforms its counterparts, while achieving state-of-the-art performance.

## 1 Introduction

Undergoing extensive pre-training on web-scale image-text pairs [1–3], vision-language models (VLMs) have demonstrated promising zero-shot generalization ability. VLMs [1, 4–7] are trained to associate images with relevant textual descriptions. However, there often exists a domain gap between pre-training data and that in domain-specific downstream tasks [8–10], especially the annotation

Method	Alignment	Visual Prompt	Textual Prompt	Avg. Acc.
CLIP [1]	Point-to-Point	-	a photo of a {class}	63.58
DCLIP [11]	Point-to-Set	-	a photo of a {class}, {description}	66.27
TPS [12]	Set-to-Set	Random Aug.	a photo of a {class}, {description}	66.95
AWT [13]	Set-to-Set	Random Aug.	a photo of a {class}, {description}	70.51
CPE (Ours)	Set-to-Set	<b>Region Selection</b> Aug.	a photo of a {synonym}, {description}	<b>72.56</b>

Table 1: **Comparison of existing CLIP-based zero-shot generalization methods from the visual-textual alignment.** Different from previous works, our CPE improves upon set-to-set alignment by incorporating constraints on visual prompts and textual prompts, while achieving higher average accuracy on 10 zero-shot image classification datasets.

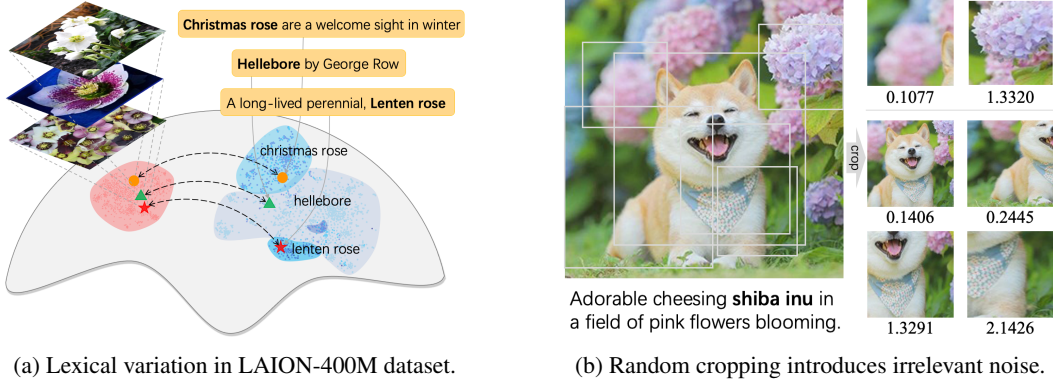


Figure 1: (a) **Lexical variation in LAION-400M dataset:** We retrieved captions and corresponding images of the concept “hellebore” from the web-scale pre-trained dataset LAION-400M [2] and visualized their CLIP embeddings. (b) **Random cropping introduces irrelevant noise:** We perform random cropping on an image of a dog and present six cropped views along with their matching entropy values with respect to all labels in the Oxford Pets.

mode of textual concepts. This intuitively leads to semantic misalignment between image and text in the feature space defined by pre-trained VLMs, limiting the zero-shot generalization ability.

To address the above issue, several promising solutions have been proposed, which can be roughly categorized into text prompting and visual-text adaptation. Specifically, text prompting, such as DCLIP [11], focus on employing large language models (LLMs) to generate multiple and more detailed textual descriptions of each category. This strategy leverages the prior knowledge embedded in LLMs, allowing the model to better capture category-specific features and improve alignment with visual content (Row 2 of Table 1). As the generated textual descriptions become more refined and comprehensive, the zero-shot performance of existing methods gradually improves. However, VLMs pre-trained on web-scale datasets inevitably face the challenge of lexical variation [14], as a single concept can be expressed using multiple synonyms. For instance, textual prompts for the concept of “hellebore” can include synonyms such as “hellebore”, “christmas rose”, and “lenten rose”. As illustrated in Figure 1a, text embeddings of synonyms are relatively far away each others, but image embeddings are close to each other in feature space. Besides, as shown in Figure 2, classification accuracy significantly changes along various selections of synonyms on Oxford Flowers, while a comprehensive textual set consistently enhances the model’s zero-shot recognition accuracy significantly. Therefore, these synonyms collectively contribute to semantic representation of one textual concept, and incomplete textual semantics will limit the zero-shot performance of VLMs.

Building upon text prompting, visual-text adaptation aims to enhance visual inputs. In contrast to aligning textual descriptions with the whole image, visual-text adaptation (such as TPS [12] and AWT [13]) randomly crop the image into multiple regions and focus on aligning specific areas with textual descriptions, thereby reducing the semantic bias that arises from global alignment (Rows 3-4 of Table 1). However, random cropping introduces irrelevant noise to the target. As shown in Figure 1b, an image of a dog might contain irrelevant and noisy elements such as a “flower” or “grass”. Previous works [12, 13, 15] have been studied to eliminate noisy regions with high image-text matching entropy, but this approach may not always be practical. An shown in Figure

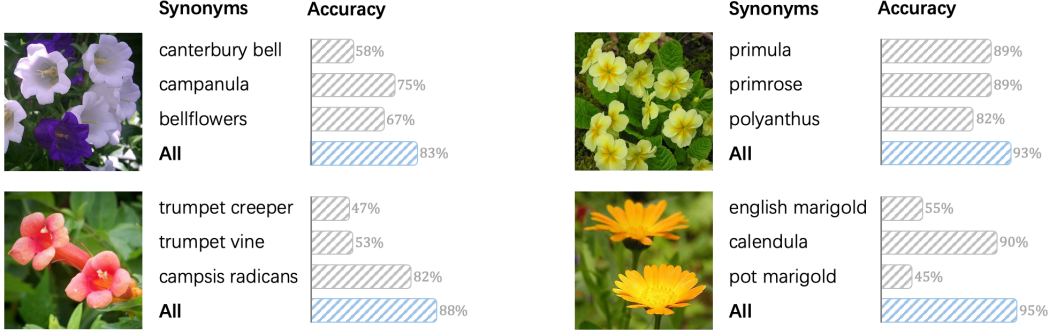


Figure 2: **Effect of synonyms selection.** We replace the given concept name (e.g., “canterbury bell”) with its synonyms (e.g., “campanula” and “bellflowers”) in the prompt template, such as “a photo of a {concept}”. Additionally, we employ prompts that include all available synonyms. We demonstrate the impact of synonym selection on classification accuracy for various Oxford Flowers concepts. Using all available synonyms yields superior performance compared to using a single synonym.

1b, two background regions (i.e., “flowers” (misclassified as “Abyssinian” and “German Shorthair”) are irrelevant to the target “Shiba Inu”, but they have lower matching entropy than some ones of the cropped regions containing the target, making them difficult to be identified as noise. In conclusion, although existing methods have shown promising results, they still face challenges of incomplete textual prompts and noisy visual prompts.

To address these challenges, we propose a novel constrained prompt enhancement (CPE) method, whose core idea is to perform a set-to-set matching between comprehensive textual prompts and compact visual prompts for improving visual-textual alignment, thereby enhancing zero-shot generalization of VLMs. To this end, our CPE method consists of two key components: Topology-Guided Synonymous Semantic Generation (TGSSG) and Category-Agnostic Discriminative Region Selection (CADRS). Specifically, our **TGSSG** first generates synonyms and descriptions for class labels by leveraging some advanced large language models (e.g., Claude [16] and GPT-4 [17]), while introducing semantic ambiguity entropy and persistent homology analysis to filter out irrelevant candidates. As such, our TGSSG constructs comprehensive textual prompts, addressing the issue that existing textual prompts cannot fully capture the intended semantics. On another hand, our **CADRS** feeds images into a pre-trained vision model (e.g., DINO [18]), and identifies the discriminative regions while filtering the irrelevant noise by performing a statistical threshold of the outputted activation maps. As such, our CADRS constructs compact visual prompts, mitigating the irrelevant and noisy views introduced by random cropping. Based on the generated comprehensive set of textual prompts and compact set of visual prompts, we introduce two set-to-set matching strategies based on test-time adaptation (TTA) and optimal transport (OT) to perform effective visual-textual alignment, namely CPE-TTA and CPE-OT. Specifically, CPE-TTA dynamically adapts text embeddings to visual content via entropy minimization during test time, and CPE-OT aligns visual and textual sets by solving a mass transportation problem with entropy-regularized cost matrices. The overview of our method is illustrated in Figure 3. To evaluate the effectiveness of our CPE method, experiments are conducted on ten zero-shot image classification tasks (i.e., Oxford Flowers [19], DTD [20], Oxford Pets [21], Stanford Cars [22], UCF101 [23], Caltech101 [24], Food101 [25], SUN397 [26], FGVC Aircraft [27], and EuroSAT [28]), five zero-shot out-of-distribution generalization tasks (e.g., ImageNet [29], ImageNet-A [30], ImageNet-V2 [31], ImageNet-R [32], and ImageNet-Sketch [33]), and three zero-shot video action recognition tasks (e.g., UCF101 [23], HMDB51 [34], and Kinetics-600 [35]). The contributions of this work are summarized as follows:

- (i) In this paper, we propose a novel constrained prompt enhancement (CPE) method, whose core idea is to perform a set-to-set matching between comprehensive textual prompts and compact visual prompts for improving visual-textual alignment of VLMs.
- (ii) To this end, our CPE presents Topology-Guided Synonymous Semantic Generation (TGSSG) and Category-Agnostic Discriminative Region Selection (CADRS) to generate comprehensive textual prompts and compact visual prompts, respectively. Subsequently, two set-to-set matching strategies

based on test-time adaptation (TTA) and optimal transport (OT) are introduced to align the enhanced textual prompts and enhanced visual prompts.

(iii) Extensive experiments demonstrate our CPE method clearly outperforms its counterparts, while achieving state-of-the-art performance.

## 2 Related Work

**Vision-language models.** Leveraging extensive pre-training on web-scale image-text pairs, vision-language models (VLMs) such as CLIP [1], ALIGN [4], SigLIP [36], and EVA-CLIP [37] embed both texts and images into a shared feature space. This facilitates the proximity of semantically similar inputs, resulting in exceptional performance across a wide range of open-ended tasks, including image classification [38–40], object detection [41–43], and video action recognition [44–46]. However, pre-trained VLMs often exhibit biases related to gender, race, and geography [14, 8], result in skewed predictions in downstream tasks. This study aims to mitigate these biases by incorporating comprehensive textual prompts and compact visual prompts within VLMs.

**Textual prompting in VLMs.** CLIP [1] suggests that placing a given concept name in human-engineered prompt templates, such as “a photo of a {class}” or “a demonstration of a {class}”, often improves zero-shot recognition performance, and highlights that the choice of prompt significantly influences the performance of downstream tasks [39, 40]. DCLIP [11] and CuPL [47] leverage the knowledge contained in LLMs, such GPT-3 [48] to automatically generate class-specific descriptions, enriching the semantic content of textual prompts and leading to more effective results. WaffleCLIP [49] and MPVR [50] further confirm that combining concept names with descriptions in prompts (e.g., “a photo of a {class}, {description}”) significantly reduces semantic bias and achieves improved performance in downstream tasks. Recent study [14] shows that replacing the given class name with its most common name in the prompt can improve zero-shot recognition for fine-grained species. In contrast, this study advocates that multiple synonyms collectively contribute to semantic representation of one textual concept.

**Visual-text adaptation in VLMs.** In contrast to focusing solely on text augmentation, visual-text adaptation aims to improve alignment by processing both visual and textual inputs. WCA [15] suggests that more detailed textual descriptions may align more accurately with specific areas of an image, enabling better cross-alignment of finer descriptions with local visual regions through random region cropping. AWT [13] formulates the matching between randomly cropped visual regions and descriptions generated by LLMs as an optimal transport problem, significantly enhancing zero-shot recognition. In comparison, test-time prompt tuning [51–54, 12] fine-tunes image or textual prompts using learnable parameters. These parameters are trained by computing the matching entropy between randomly cropped visual regions and textual prompts, thus improving the alignment between the image and text. This study argues that filtering out irrelevant noise regions using the inherent knowledge of images aids in improving alignment between images and texts.

## 3 Proposed Method

As illustrated in Figure 3, our CPE method consists of two key components: Topology-Guided Synonymous Semantic Generation (TGSSG) and Category-Agnostic Discriminative Region Selection (CADRS). For each candidate class names, synonyms and descriptions are generated using large language models (LLMs) and input into the TGSSG to construct a comprehensive textual set. Given a test image, the activation map is extracted by the pre-trained vision model and fed into the CADRS to build a compact visual set. The set-to-set visual-textual matching is then applied to measure the predicted probability of the visual set corresponding to each class’s textual set. A detailed description of these three modules is provided below.

### 3.1 Topology-Guided Synonymous Semantic Generation

Textually, zero-shot generalization in VLMs generally is affected by the issue on lexical variation of textual prompts. Recent works [50, 13] propose to use two-stage generation for textual descriptions via LLMs, which allow more nuanced semantic information and lead to competitive performance.

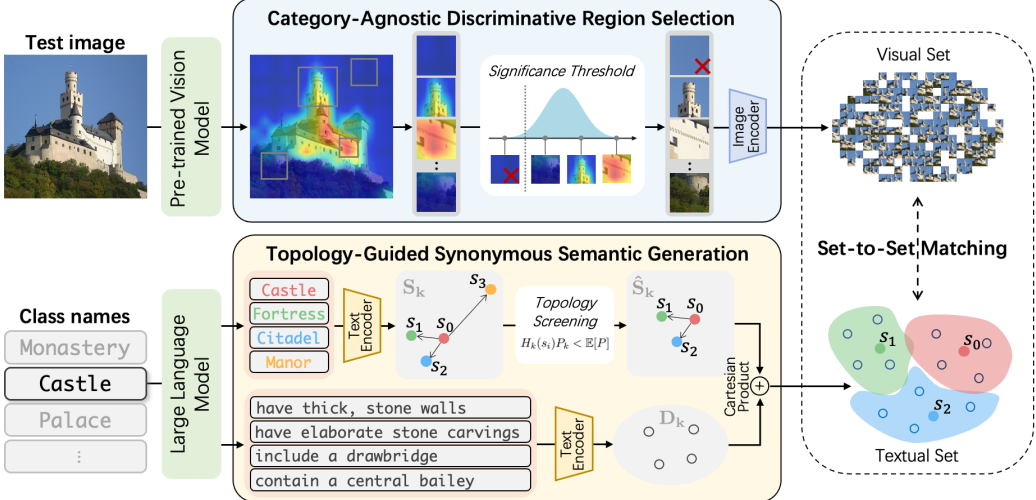


Figure 3: **Overall architecture of CPE.** For each candidate class, synonyms and descriptions are generated using LLMs and processed by the Topology-Guided Synonymous Semantic Generation to form a comprehensive textual set. A test image is passed through the pre-trained vision model to obtain an activation map, which is then processed by the Category-Agnostic Discriminative Region Selection to create a compact visual set. The Set-to-Set Visual-Textual Matching evaluates the predicted probability of the visual set aligning with each class’s textual set.

However, existing methods focus solely on the given labels, while we argue that synonyms with related semantic contribute to a more comprehensive semantic representation of a concept (Figure 1a). To address this issue, we propose Topology-Guided Synonymous Semantic Generation (TGSSG), which utilizes LLMs to generate synonyms and descriptions for category names. To mitigate noise caused by hallucinations in the LLM outputs, we filter irrelevant candidates using semantic ambiguity entropy and persistent homology analysis, thereby constructing comprehensive textual prompts sets.

For one of the candidate class names  $C_k$ , we first prompt an off-the-shelf LLM (e.g., Claude [16]) as: "Tell me in five words or less what are some common ways of referring to {class\\_name}?" It generates synonyms set  $S_k = \{s_0, s_1, \dots\}$  for the class name  $C_k$ . However, hallucinations in LLMs often lead to suboptimal results [55, 56]. To ensure semantic consistency with the target class, we process the generated synonym set by analyzing its topology and removing outlier synonyms. Specifically, we map all synonyms to a feature set  $F_k = \{f_0, f_1, \dots\}$  using the CLIP text encoder and compute the semantic ambiguity entropy:

$$H_k(s_i) = - \sum_{j \neq i} d(f_i, f_j) \log d(f_i, f_j), \quad (1)$$

where  $d(\cdot, \cdot)$  denotes the cosine similarity distance and  $H_k(s_i)$  reflects the degree of semantic deviation of  $s_i$  within the set  $S_k$ . Next, we construct the Vietoris-Rips complex [57, 58] of the synonym feature set  $F_k$  and compute its persistent homology persistence  $P_k$ , which characterizes the topological compactness of the set. Finally, we retain synonyms that satisfy the condition:

$$\hat{S}_k = \{s_i \mid H_k(s_i)P_k < \mathbb{E}[P], s_i \in S_k\}, \quad (2)$$

where  $\mathbb{E}[P]$  represents the mean of persistence  $P_k$  across all classes. The combined entropy and topological persistence filter out synonyms that deviate significantly from the primary semantic distribution, optimizing the reasonableness of semantic expression. Subsequently, we employ a two-step dataset-aware prompting strategy to generate a tailored description set  $D_k$  for each class label  $C_k$  following [50, 13]. By combining this description set  $D_k$  with the synonyms set  $\hat{S}_k$  through the template "a photo of a {synonym}, {description}" and encoding them with the CLIP text encoder, we obtain the comprehensive textual prompts set  $T_k$ .

### 3.2 Category-Agnostic Discriminative Region Selection

Visually, it is commonly assumed that diverse multi-scale image views are more suited for fine text alignment, compared to the whole image [13, 15]. However, random image cropping and flipping strategy used in existing works [13, 15] often introduce irrelevant noise. Although integration of cross-modal matching entropy can mitigate effect of these noise, it hardly fully eliminates irrelevant noise, thereby bringing the side effect on performance of text-image alignment (Figure 1b). To address the issue of irrelevant visual noise introduced by random cropping, we propose Category-Agnostic Discriminative Region Selection (CADRS), which identifies discriminative regions through important activations and filters out background noise using statistical thresholds, thereby generating a compact visual prompts set.

Formally, given a test image  $X \in \mathbb{R}^{3 \times H \times W}$ , we utilize a pre-trained vision model (e.g., DINO [18]) to generate a category-agnostic attention map  $A \in \mathbb{R}^{H \times W}$ . Both the test image  $X$  and the attention map  $A$  undergo the same standard data augmentations, including random resized cropping and random flipping, producing augmented views  $\{X_n\}_{n=1}^N$  and  $\{A_n\}_{n=1}^N$ , respectively. In practice, irrelevant noise views typically correspond to background regions, where activation values in the attention map are expected to be low. We hypothesize that these regions can be identified through the statistical properties of the attention map’s activations. Specifically, we model the average activation values across all views  $\{A_n\}_{n=1}^N$  as a Gaussian distribution,  $N(\mu, \sigma^2)$ , where  $\mu$  and  $\sigma$  represent the mean and standard deviation of the activation values, respectively. This model allows for the identification of views with low activations, which are often associated with irrelevant background noise. To quantitatively determine which views to discard, we apply a significance threshold using a two-standard deviation rule [59]. Specifically, views with activation values below  $\mu - 2\sigma$  are considered outliers and discarded, while those above this threshold are retained. The remaining indices  $\mathbf{I} = \{i \mid \mathbb{E}[A_i] > \mu - 2\sigma\}$ , where  $\mathbb{E}[A_i]$  denotes the average activation of  $A_i$ , resulting in a set of selected views that are considered to contain meaningful information for text-image alignment. Together with the original image  $X$ , the compact visual prompts set is constructed as follows:

$$\mathbf{V} = \{\phi(x) \mid x \in \{X\} \cup \{X_i\}_{i \in \mathbf{I}}\}, \quad (3)$$

where  $\phi$  donates the CLIP image encoder. This method ensures that only the most relevant image regions, based on statistical significance, are retained for downstream tasks, thus enhancing the robustness and efficiency of text-image alignment.

### 3.3 Set-to-set Visual-textual Matching

To achieve precise matching between our constructed comprehensive textual prompts and compact visual prompts for zero-shot prediction, we introduce two set-to-set matching strategies based on test-time adaptation (TTA) and optimal transport (OT), resulting in CPE-TTA and CPE-OT methods. Note that the pipelines of CPE-TTA and CPE-OT methods are illustrated in Figure 5 in the Appendix.

**CPE-TTA.** Test-time adaptation (TTA) enables dynamic adaptation of textual prompts to better align with visual content during inference. In our approach, TTA is used to dynamic adapt the matching between the visual set and textual set constructed in the previous steps. Specifically, for a test image, we replace random cropping in [12] with the compact multi-scale visual set  $\mathbf{V}$ . For each category’s comprehensive textual set  $\mathbf{T}_k$ , we apply a learnable vector  $l_k$  to uniformly shift the embeddings in the set at the channel level, as described in [12]. Next, we calculate predicted probability of each view in the image set  $v_i \in \mathbf{V}$  with respect to each textual set  $\mathbf{T}_k$  as

$$p(k \mid v_i) = \frac{\exp((\mathbb{E}[\mathbf{T}_k] + l_k)^\top v_i / \tau)}{\sum_j \exp((\mathbb{E}[\mathbf{T}_j] + l_j)^\top v_i / \tau)} \quad (4)$$

where  $\mathbb{E}[\mathbf{T}_k]$  represents the average embedding of the textual set  $\mathbf{T}_k$  and  $\tau$  denotes the temperature scalar. Similar to [12], we select the  $m$  distributions with lowest entropy of the batch and take the average. By minimizing the entropy of this marginal distribution, we update  $l_k$  via a single-step gradient descent. During inference, the similarity between the center of the image set and the center of the shifted textual set is measured to perform zero-shot prediction.

**CPE-OT.** Optimal Transport (OT), originating from the Monge problem [60], provides a framework to measure similarity between distributions by finding the most efficient way to transform one

distribution into another. In our context, we treat the visual set  $\mathbf{V}$  and textual set  $\mathbf{T}_k$  as two discrete distributions. Mathematically, we model each element in both sets as a mass located at its embedding position:

$$\alpha = \sum_{i=1}^N \mathbf{a}_i \delta_{v_i} \quad \text{and} \quad \beta^k = \sum_{j=1}^M \mathbf{b}_j \delta_{t_j^k}, \quad (5)$$

where  $N$  and  $M$  are number of samples in  $\mathbf{V}$  and  $\mathbf{T}_k$ ,  $\delta$  denotes the Dirac function.  $\mathbf{a}_i$  and  $\mathbf{b}_j$  are the entropy-based importance weight of each element introduced in [13]. The transportation cost between any element  $v_i$  from visual set  $\mathbf{V}$  and any element  $t_j^k$  from textual set  $\mathbf{T}_k$  is quantified using the cosine distance between their embeddings. Therefore, we can adopt the Kantorovich relaxation [61] to form the optimal transport problem between the two sets as:

$$\mathbf{P}_k^* = \arg \min_{\mathbf{P} \in \mathbb{R}^{M \times N}} \sum_{i=1}^M \sum_{j=1}^N \mathbf{C}_{ij} \mathbf{P}_{ij} \quad \text{s.t.} \quad \mathbf{P} \mathbf{1}_M = \mathbf{a} \quad \text{and} \quad \mathbf{P}^T \mathbf{1}_N = \mathbf{b}. \quad (6)$$

Here  $\mathbf{C} \in \mathbb{R}^{M \times N}$  defines the cost matrix. Eq. 6 can be efficiently approximated using the Sinkhorn Algorithm [62]. Consequently, the classification probability can be expressed as:

$$p(k \mid \mathbf{V}) = \frac{\exp(\mathbf{P}_k^*/\tau)}{\sum_j \exp(\mathbf{P}_j^*/\tau)}, \quad (7)$$

where  $\mathbf{P}_k^*$  represents the optimal transport cost from  $\mathbf{V}$  to  $\mathbf{T}_k$  and  $\tau$  denotes the temperature scalar.

## 4 Experiments

### 4.1 Implementation Details

In this section, we utilize CLIP ViT-B/16 as the basic model for comparing all methods. To generate synonyms, we leverage the public web API of Claude-3.5-Sonnet [16] by setting the number of synonyms  $M^*$  to 5. Descriptions are generated using a script based on the code repository provided in [50, 13] by using the identical configurations. The number of candidate augmented images  $N^*$  is initialized by 100. Activation maps are generated using Attention Rollout [63] on DINO [18]. A detailed discussion of the hyperparameters is provided in the ablation study. All experiments are conducted in PyTorch and run on a PC with dual NVIDIA RTX 3090 GPUs.

### 4.2 Zero-Shot Image Classification

We conduct zero-shot image classification on 10 widely used datasets: Oxford Flowers [19], Oxford Pets [21], Stanford Cars [22], Food101 [25], and FGVC Aircraft [27] for fine-grained classification, DTD [20] for texture classification, UCF101 [23] for action recognition, Caltech101 [24] for generic object recognition, SUN397 [26] for scene recognition, and EuroSAT [28] for satellite recognition. For a thorough evaluation, we primarily compare four distinct categories of zero-shot methods: (1) Baseline: The standard CLIP model [1] based on the ViT-B/16 architecture, using a conventional prompt template. (2) Prompt learning: Methods those incorporate additional data for model fine-tuning, such as CoOp [39], CoCoOp [40], MaPLe [64], PLOT++ [65], POMP [66], and ProVP-Ref [67]. (3) Test-time prompt tuning: Methods those optimize visual or textual prompts during inference, including TPT [51], DiffTPT [52], TTL [54], PromptAlign [53], and TPS [12]. (4) Prompt enhancement: Methods those leverage LLMs to generate enriched prompts, such as CuPL [47], DCLIP [11], WaffleCLIP [49], SuS-X [68], REAL [14], MPVR [50], and AWT [13].

The compared results are given in Table 2, from it we can draw the following conclusions. (1) Compared to prompt learning methods that perform well in few-shot scenarios, our method achieves a more than 6% improvement in average accuracy across 10 datasets, even though prompt learning methods fine-tune with additional data from the ImageNet dataset. This demonstrates that, unlike few-shot scenarios in VLMs, additional data fine-tuning is not necessary for zero-shot generalization. (2) In comparison to test-time prompt tuning methods, our CPE-TTA achieves an average accuracy 2.87% higher than the previous best result, TPS. This indicates that enhancing both visual and textual prompts is equally effective for test-time prompt tuning. (3) Compared to prompt enhancement methods, our CPE-OT further enhances the prompts, outperforming the previous best, AWT, by

	<i>Flowers</i>	<i>DTD</i>	<i>Pets</i>	<i>Cars</i>	<i>UCF</i>	<i>CalTech</i>	<i>Food</i>	<i>SUN</i>	<i>Aircraft</i>	<i>SAT</i>	<i>Avg.</i>
CLIP [1]	67.44	44.27	88.25	65.48	65.13	93.35	83.65	62.59	23.67	42.01	63.58
CoOp [39]	68.71	41.92	89.14	64.51	66.55	93.70	85.30	64.15	18.47	46.39	63.88
CoCoOp [40]	71.88	45.73	90.14	65.32	68.21	94.43	86.06	67.36	22.94	45.37	65.74
MaPLe [64]	72.23	46.49	90.49	65.57	68.69	93.53	86.20	67.01	24.74	48.06	66.30
PLOT++ [65]	69.10	38.42	90.49	61.20	68.94	91.32	86.07	61.59	24.84	49.90	64.19
POMP [66]	72.72	44.44	89.05	66.70	68.44	94.65	86.28	67.27	25.47	52.65	66.77
ProVP-Ref [67]	71.62	45.97	91.58	65.29	67.72	93.79	86.17	66.29	24.51	51.95	66.49
TPT [51]	68.98	47.75	87.79	66.87	68.04	94.16	84.67	65.50	24.78	42.44	65.10
DiffTPT [52]	70.10	47.00	88.22	67.01	68.22	92.49	<b>87.23</b>	65.74	25.60	43.13	65.47
TTL [54]	70.48	46.69	88.72	67.96	69.20	93.63	85.05	66.32	23.82	42.02	65.39
PromptAlign [53]	72.39	47.24	90.76	68.50	69.47	94.01	86.65	67.54	24.80	47.86	66.92
TPS [12]	71.54	50.47	87.35	69.06	71.00	95.09	85.23	68.98	26.34	44.48	<b>66.95</b>
CuPL [47]	71.30	44.56	89.13	65.29	66.83	92.98	86.11	62.59	24.90	47.84	65.15
DCLIP [11]	70.85	44.98	88.85	64.08	67.12	94.60	85.05	67.99	24.30	54.84	66.27
WaffleCLIP [49]	72.35	45.21	89.95	63.57	67.19	94.02	86.68	67.23	25.39	55.07	66.67
SuS-X [68]	73.81	54.55	90.57	66.13	66.59	93.96	86.08	67.73	28.68	57.49	68.56
REAL [14]	73.20	51.12	91.41	66.45	65.40	90.22	83.71	62.61	24.69	54.44	66.33
MPVR [50]	76.90	56.10	89.90	65.40	70.90	94.10	86.40	68.80	28.00	59.60	69.61
AWT [13]	75.07	55.56	92.53	69.93	72.51	95.54	85.54	70.58	29.22	58.61	<b>70.51</b>
CPE-TTA	77.83	55.79	89.29	66.96	72.51	95.25	85.86	70.21	29.70	54.81	69.82 <sup>±2.87</sup>
<b>CPE-OT</b>	<b>84.25</b>	<b>57.80</b>	<b>92.59</b>	<b>70.17</b>	<b>73.06</b>	<b>95.78</b>	86.06	<b>70.65</b>	<b>32.67</b>	<b>62.59</b>	<b>72.56<sup>±2.05</sup></b>

Table 2: **Zero-shot image classification.** We report top-1 accuracy (%) for each dataset. The best accuracies are highlighted in **bold**, and the average for comparison with CPE is presented in **blue**.

	<b>IN-1k</b>	<b>IN-A</b>	<b>IN-V2</b>	<b>IN-R</b>	<b>IN-K</b>	<b>OOD</b>		<b>UCF</b>	<b>HM</b>	<b>K600</b>
CLIP [1]	66.74	47.74	60.75	73.98	46.13	57.15	ActionCLIP [44]	77.5	48.2	62.5
TPT [51]	68.98	54.77	63.45	77.06	47.94	60.81	X-CLIP [69]	72.0	44.6	65.2
DiffTPT [52]	70.30	55.68	65.10	75.00	46.80	60.65	AIM [70]	79.4	50.3	66.7
TPS [12]	71.45	<b>60.61</b>	64.91	80.20	50.88	64.15	ST-Adapter [71]	77.6	51.1	60.2
CuPL [47]	69.62	50.72	63.27	77.05	49.02	60.02	Vita-CLIP [72]	75.0	48.6	67.4
DCLIP [11]	68.55	49.07	61.80	75.13	47.97	58.49	ViFi-CLIP [73]	76.8	51.3	71.2
WaffleCLIP [49]	68.81	50.78	62.54	77.49	49.10	59.98	AdaptFormer [74]	80.3	51.0	67.0
REAL [14]	68.50	50.04	61.97	77.69	48.19	59.47	Open-VCLIP [45]	83.4	53.9	73.0
MPVR [50]	69.70	-	63.40	78.20	50.60	-	FROSTER [46]	84.8	54.8	74.8
AWT [13]	71.32	60.33	65.15	80.64	51.60	64.43	AWT [13]	85.2	57.2	76.1
<b>CPE-OT</b>	<b>71.74</b>	60.12	<b>65.48</b>	<b>80.69</b>	<b>52.76</b>	<b>64.76</b>	<b>CPE-OT</b>	<b>85.7</b>	<b>57.9</b>	<b>77.3</b>

Table 3: **Zero-shot out-of-distribution generalization.**

Table 4: **ZS video recognition.**

2.05% in average accuracy. This suggests that comprehensive textual prompts and compact visual prompts can significantly improve zero-shot recognition. (4) Our method outperforms all existing approaches with a significant advantage, achieving state-of-the-art performance in 9 out of 10 datasets, demonstrating the superiority of the proposed method.

### 4.3 Zero-Shot Out-of-Distribution Generalization

We assess the domain generalization ability of our CPE-OT method on 5 natural distribution datasets including ImageNet [29] and its out-of-distribution variants ImageNet-A [30], ImageNet-V2 [31], ImageNet-R [32], and ImageNet-Sketch [33]. Table 3 compares the results of various methods on ImageNet and four OOD benchmarks, where we can observe that (1) our CPE-OT method outperforms all existing approaches on ImageNet, achieving an improvement of 0.42% over the recently proposed state-of-the-art (AWT). (2) Besides, our CPE-OT achieves the best performance on three out of four

(a) Effect of key components			(b) Effect of number $M^*$			(c) Effect of number $N^*$		
Step	IN-1k	Avg.(10)	$M^*$	IN-1k	Avg.(10)	$N^*$	IN-1k	Avg.(10)
AWT (baseline)	71.28	70.44	1	68.84	70.62	25	71.55	72.39
+V	71.35	70.49	2	70.72	71.67	50	71.43	72.30
+T w/o filter	71.46	71.81	3	71.06	72.40	100	<b>71.74</b>	<b>72.56</b>
+T	71.58	72.33	4	71.37	72.52	150	71.73	72.43
+V+T	<b>71.74</b>	<b>72.56</b>	5	<b>71.74</b>	<b>72.56</b>	200	71.69	72.41
			6	71.68	72.53			

Table 5: **Ablation study** across ImageNet and 10 image classification datasets. The default configuration is colored gray. T and V indicates textual and visual prompt enhancement, respectively.

OOD datasets, and obtains the highest average score, surpassing the previous best results by 0.33%. These improvement over AWT owes to our constrained visual and textual prompt enhancement helps to handle complex OOD data. (3) Note that our CPE-OT achieves a substantial improvement of 1.16% on ImageNet-Sketch, owing to the uniform backgrounds and well-defined object contours in hand-drawn sketches, which facilitate the identification and localization of discriminative regions. In contrast, performance of CPE-OT on ImageNet-A is modest, which may be caused by that natural adversarial examples introduce distracting artifacts that hinder the model’s discrimination. These results above clearly demonstrate that our CPE-OT is well generalized to OOD settings.

#### 4.4 Zero-Shot Video Recognition

Following the setup of AWT [13], we evaluate the zero-shot generalization capability of our method for video action recognition using three widely used datasets: UCF101 [23], HMDB51 [34], and Kinetics-600 [35]. For each dataset, we assess the model performance using three official or commonly used splits and report the average result across all splits. To capture temporal dynamics in visual features, we also follow Open-VCLIP [45] to use neighbor-frame attention and fine-tune CLIP on Kinetics-400. Textual prompt enhancement is the same for zero-shot image classification task.

In Table 4, we compare our method with existing CLIP-based zero-shot video action recognition approaches [44, 69–74, 45, 46]. According to the results, we have two observations. (1) Although our method is not specifically designed for video tasks, it achieves state-of-the-art performance, surpassing the previous best AWT by 0.5%, 0.7% and 1.2% on UCF101, HMDB51 and Kinetics-600, respectively. These results demonstrate that our approach is effective for video understanding tasks. (2) Compared to AWT, our method improves zero-shot video recognition solely by constructing comprehensive textual prompts set, demonstrating the significance of textual semantics on video understanding.

#### 4.5 Ablation Study

**Effect of key components.** Table 5a presents an analysis for effect of key components on our method. Initially, we separately enhance the textual and visual components. The results (rows 2 and 4) indicate that enhancing the textual prompts yields more significant improvements than enhancing the visual prompts. Additionally, the results (rows 3 and 4) suggest that filtering the generated synonym sets is essential. Finally, we enhance both the textual and the visual prompts simultaneously, and the results (row 4) demonstrate that this combination produces the best performance.

**Effect of hyperparameters.** Table 5b and 5c present study on effect of hyperparameters in textual and visual prompts, including number of **generated synonyms**  $M^*$  and number of **augmented image views**  $N^*$ . For the number of generated synonyms, performance improves along the increased number and stabilizes at  $M^* = 5$ , indicating small number of synonyms is insufficient to capture the full textual semantic. For number of augmented image views, we found that augmentation of  $N^* = 100$  yields the best results. Particularly, too few augmentations fail to cover all useful characteristics, while too many augmentations will introduce excessive noise.

## 5 Conclusions

In this paper, we proposed a constrained prompt enhancement method to improve zero-shot generalization of VLMs, whose core idea is to perform a set-to-set matching between comprehensive textual prompts and compact visual prompts for improving visual-textual alignment. To this end, a topology-guided synonymous semantic generation and a category-agnostic discriminative region selection are presented to construct comprehensive textual prompts and generated compact visual prompts, respectively. Subsequently, two set-to-set matching strategies are introduced to achieve effective visual-textual alignment. Extensive experiments demonstrate the effectiveness of our approach. We hope our analysis on completeness of textual prompts and compactness of visual prompts can encourage further research on improving generalization of VLMs.

## References

- [1] Alec Radford, Jong Wook Kim, Chris Hallacy, Aditya Ramesh, Gabriel Goh, Sandhini Agarwal, Girish Sastry, Amanda Askell, Pamela Mishkin, Jack Clark, et al. Learning transferable visual models from natural language supervision. In *International Conference on Machine Learning*, pages 8748–8763. PMLR, 2021.
- [2] Christoph Schuhmann, Richard Vencu, Romain Beaumont, Robert Kaczmarczyk, Clayton Mullis, Aarush Katta, Theo Coombes, Jenia Jitsev, and Aran Komatsuzaki. Laion-400m: Open dataset of clip-filtered 400 million image-text pairs. *arXiv preprint arXiv:2111.02114*, 2021.
- [3] Christoph Schuhmann, Romain Beaumont, Richard Vencu, Cade Gordon, Ross Wightman, Mehdi Cherti, Theo Coombes, Aarush Katta, Clayton Mullis, Mitchell Wortsman, et al. Laion-5b: An open large-scale dataset for training next generation image-text models. *NeurIPS*, 35:25278–25294, 2022.
- [4] Chao Jia, Yafei Yang, Ye Xia, Yi-Ting Chen, Zarana Parekh, Hieu Pham, Quoc Le, Yun-Hsuan Sung, Zhen Li, and Tom Duerig. Scaling up visual and vision-language representation learning with noisy text supervision. In *International Conference on Machine Learning*, pages 4904–4916. PMLR, 2021.
- [5] Xiaohua Zhai, Xiao Wang, Basil Mustafa, Andreas Steiner, Daniel Keysers, Alexander Kolesnikov, and Lucas Beyer. Lit: Zero-shot transfer with locked-image text tuning. In *CVPR*, pages 18123–18133, 2022.
- [6] Yunhao Ge, Jiashu Xu, Brian Nlong Zhao, Neel Joshi, Laurent Itti, and Vibhav Vineet. Dall-e for detection: Language-driven compositional image synthesis for object detection. *arXiv preprint arXiv:2206.09592*, 2022.
- [7] Aditya Ramesh, Mikhail Pavlov, Gabriel Goh, Scott Gray, Chelsea Voss, Alec Radford, Mark Chen, and Ilya Sutskever. Zero-shot text-to-image generation. In *International Conference on Machine Learning*, pages 8821–8831. PMLR, 2021.
- [8] Ninareh Mehrabi, Fred Morstatter, Nripsuta Saxena, Kristina Lerman, and Aram Galstyan. A survey on bias and fairness in machine learning. *ACM computing surveys (CSUR)*, 54(6):1–35, 2021.
- [9] Sachit Menon, Ishaan Preetam Chandratreya, and Carl Vondrick. Task bias in vision-language models. *arXiv preprint arXiv:2212.04412*, 2022.
- [10] Sandhini Agarwal, Gretchen Krueger, Jack Clark, Alec Radford, Jong Wook Kim, and Miles Brundage. Evaluating clip: towards characterization of broader capabilities and downstream implications. *arXiv preprint arXiv:2108.02818*, 2021.
- [11] Sachit Menon and Carl Vondrick. Visual classification via description from large language models. *ICLR*, 2022.
- [12] Elaine Sui, Xiaohan Wang, and Serena Yeung-Levy. Just shift it: Test-time prototype shifting for zero-shot generalization with vision-language models. *arXiv preprint arXiv:2403.12952*, 2024.
- [13] Yuhan Zhu, Yuyang Ji, Zhiyu Zhao, Gangshan Wu, and Limin Wang. Awt: Transferring vision-language models via augmentation, weighting, and transportation. *NeurIPS*, 2024.
- [14] Shubham Parashar, Zhiqiu Lin, Tian Liu, Xiangjue Dong, Yanan Li, Deva Ramanan, James Caverlee, and Shu Kong. The neglected tails in vision-language models. In *CVPR*, pages 12988–12997, 2024.
- [15] Jinhao Li, Haopeng Li, Sarah Erfani, Lei Feng, James Bailey, and Feng Liu. Visual-text cross alignment: Refining the similarity score in vision-language models. *arXiv preprint arXiv:2406.02915*, 2024.
- [16] Anthropic. The claude 3 model family: Opus, sonnet, haiku, 2024.
- [17] Josh Achiam, Steven Adler, Sandhini Agarwal, Lama Ahmad, Ilge Akkaya, Florencia Leoni Aleman, Diogo Almeida, Janko Altenschmidt, Sam Altman, Shyamal Anadkat, et al. Gpt-4 technical report. *arXiv preprint arXiv:2303.08774*, 2023.

[18] Mathilde Caron, Hugo Touvron, Ishan Misra, Hervé Jégou, Julien Mairal, Piotr Bojanowski, and Armand Joulin. Emerging properties in self-supervised vision transformers. In *ICCV*, pages 9650–9660, 2021.

[19] Maria-Elena Nilsback and Andrew Zisserman. Automated flower classification over a large number of classes. In *Indian Conference on Computer Vision, Graphics and Image Processing*, pages 722–729, 2008.

[20] Mircea Cimpoi, Subhransu Maji, Iasonas Kokkinos, Sammy Mohamed, and Andrea Vedaldi. Describing textures in the wild. In *CVPR*, pages 3606–3613, 2014.

[21] Omkar M Parkhi, Andrea Vedaldi, Andrew Zisserman, and CV Jawahar. Cats and dogs. In *CVPR*, pages 3498–3505, 2012.

[22] Jonathan Krause, Michael Stark, Jia Deng, and Li Fei-Fei. 3d object representations for fine-grained categorization. In *ICCV*, pages 554–561, 2013.

[23] K Soomro. Ucf101: A dataset of 101 human actions classes from videos in the wild. *arXiv preprint arXiv:1212.0402*, 2012.

[24] Li Fei-Fei, Rob Fergus, and Pietro Perona. Learning generative visual models from few training examples: An incremental bayesian approach tested on 101 object categories. In *CVPR Workshop*, pages 178–178, 2004.

[25] Lukas Bossard, Matthieu Guillaumin, and Luc Van Gool. Food-101–mining discriminative components with random forests. In *ECCV*, pages 446–461, 2014.

[26] Jianxiong Xiao, James Hays, Krista A Ehinger, Aude Oliva, and Antonio Torralba. Sun database: Large-scale scene recognition from abbey to zoo. In *2010 IEEE Computer Society Conference on Computer Vision and Pattern Recognition*, pages 3485–3492. IEEE, 2010.

[27] Subhransu Maji, Esa Rahtu, Juho Kannala, Matthew Blaschko, and Andrea Vedaldi. Fine-grained visual classification of aircraft. *arXiv preprint arXiv:1306.5151*, 2013.

[28] Patrick Helber, Benjamin Bischke, Andreas Dengel, and Damian Borth. Eurosat: A novel dataset and deep learning benchmark for land use and land cover classification. *IEEE Journal of Selected Topics in Applied Earth Observations and Remote Sensing*, 12(7):2217–2226, 2019.

[29] Jia Deng, Wei Dong, Richard Socher, Li-Jia Li, Kai Li, and Li Fei-Fei. Imagenet: A large-scale hierarchical image database. In *CVPR*, pages 248–255. Ieee, 2009.

[30] Dan Hendrycks, Kevin Zhao, Steven Basart, Jacob Steinhardt, and Dawn Song. Natural adversarial examples. In *CVPR*, pages 15262–15271, 2021.

[31] Benjamin Recht, Rebecca Roelofs, Ludwig Schmidt, and Vaishaal Shankar. Do imagenet classifiers generalize to imagenet? In *International Conference on Machine Learning*, pages 5389–5400. PMLR, 2019.

[32] Dan Hendrycks, Steven Basart, Norman Mu, Saurav Kadavath, Frank Wang, Evan Dorundo, Rahul Desai, Tyler Zhu, Samyak Parajuli, Mike Guo, et al. The many faces of robustness: A critical analysis of out-of-distribution generalization. In *ICCV*, pages 8340–8349, 2021.

[33] Haohan Wang, Songwei Ge, Zachary Lipton, and Eric P Xing. Learning robust global representations by penalizing local predictive power. *NeurIPS*, 32, 2019.

[34] Hildegard Kuehne, Hueihan Jhuang, Estíbaliz Garrote, Tomaso Poggio, and Thomas Serre. Hmdb: a large video database for human motion recognition. In *ICCV*, pages 2556–2563. IEEE, 2011.

[35] Joao Carreira, Eric Noland, Andras Banki-Horvath, Chloe Hillier, and Andrew Zisserman. A short note about kinetics-600. *arXiv preprint arXiv:1808.01340*, 2018.

[36] Xiaohua Zhai, Basil Mustafa, Alexander Kolesnikov, and Lucas Beyer. Sigmoid loss for language image pre-training. In *ICCV*, pages 11975–11986, 2023.

[37] Quan Sun, Yuxin Fang, Ledell Wu, Xinlong Wang, and Yue Cao. Eva-clip: Improved training techniques for clip at scale. *arXiv preprint arXiv:2303.15389*, 2023.

[38] Boyi Li, Kilian Q Weinberger, Serge Belongie, Vladlen Koltun, and René Ranftl. Language-driven semantic segmentation. *arXiv preprint arXiv:2201.03546*, 2022.

[39] Kaiyang Zhou, Jingkang Yang, Chen Change Loy, and Ziwei Liu. Learning to prompt for vision-language models. *IJCV*, 130(9):2337–2348, 2022.

[40] Kaiyang Zhou, Jingkang Yang, Chen Change Loy, and Ziwei Liu. Conditional prompt learning for vision-language models. In *CVPR*, pages 16816–16825, 2022.

[41] C Feng, Y Zhong, Z Jie, X Chu, H Ren, X Wei, W Xie, and L Promptdet Ma. Towards open-vocabulary detection using uncurated images. In *ECCV*, pages 23–27, 2022.

[42] Xiuye Gu, Tsung-Yi Lin, Weicheng Kuo, and Yin Cui. Zero-shot detection via vision and language knowledge distillation. *arXiv preprint arXiv:2104.13921*, 2(3):4, 2021.

[43] Yu Du, Fangyun Wei, Zihe Zhang, Miaojing Shi, Yue Gao, and Guoqi Li. Learning to prompt for open-vocabulary object detection with vision-language model. In *CVPR*, pages 14084–14093, 2022.

[44] Mengmeng Wang, Jiazhen Xing, and Yong Liu. Actionclip: A new paradigm for video action recognition. *arXiv preprint arXiv:2109.08472*, 2021.

[45] Zejia Weng, Xitong Yang, Ang Li, Zuxuan Wu, and Yu-Gang Jiang. Open-vclip: Transforming clip to an open-vocabulary video model via interpolated weight optimization. In *International Conference on Machine Learning*, pages 36978–36989, 2023.

[46] Xiaohu Huang, Hao Zhou, Kun Yao, and Kai Han. Froster: Frozen clip is a strong teacher for open-vocabulary action recognition. *arXiv preprint arXiv:2402.03241*, 2024.

[47] Sarah Pratt, Ian Covert, Rosanne Liu, and Ali Farhadi. What does a platypus look like? generating customized prompts for zero-shot image classification. In *ICCV*, pages 15691–15701, 2023.

[48] Tom Brown, Benjamin Mann, Nick Ryder, Melanie Subbiah, Jared D Kaplan, Prafulla Dhariwal, Arvind Neelakantan, Pranav Shyam, Girish Sastry, Amanda Askell, et al. Language models are few-shot learners. *NeurIPS*, 33:1877–1901, 2020.

[49] Karsten Roth, Jae Myung Kim, A Koepke, Oriol Vinyals, Cordelia Schmid, and Zeynep Akata. Waffling around for performance: Visual classification with random words and broad concepts. In *ICCV*, pages 15746–15757, 2023.

[50] M Jehanzeb Mirza, Leonid Karlinsky, Wei Lin, Sivan Doveh, Jakub Micorek, Mateusz Kozinski, Hilde Kuhene, and Horst Possegger. Meta-prompting for automating zero-shot visual recognition with llms. In *ECCV*, pages 1–30, 2024.

[51] Manli Shu, Weili Nie, De-An Huang, Zhiding Yu, Tom Goldstein, Anima Anandkumar, and Chaowei Xiao. Test-time prompt tuning for zero-shot generalization in vision-language models. *NeurIPS*, 35: 14274–14289, 2022.

[52] Chun-Mei Feng, Kai Yu, Yong Liu, Salman Khan, and Wangmeng Zuo. Diverse data augmentation with diffusions for effective test-time prompt tuning. In *ICCV*, pages 2704–2714, 2023.

[53] Jameel Abdul Samadh, Mohammad Hanan Gani, Noor Hussein, Muhammad Uzair Khattak, Muhammad Muzammal Naseer, Fahad Shahbaz Khan, and Salman H Khan. Align your prompts: Test-time prompting with distribution alignment for zero-shot generalization. *NeurIPS*, 36, 2024.

[54] Raza Imam, Hanan Gani, Muhammad Huzaifa, and Karthik Nandakumar. Test-time low rank adaptation via confidence maximization for zero-shot generalization of vision-language models. In *2025 IEEE/CVF Winter Conference on Applications of Computer Vision (WACV)*, pages 5449–5459. IEEE, 2025.

[55] Yue Zhang, Yafu Li, Leyang Cui, Deng Cai, Lemao Liu, Tingchen Fu, Xinting Huang, Enbo Zhao, Yu Zhang, Yulong Chen, et al. Siren’s song in the ai ocean: a survey on hallucination in large language models. *arXiv preprint arXiv:2309.01219*, 2023.

[56] Lei Huang, Weijiang Yu, Weitao Ma, Weihong Zhong, Zhangyin Feng, Haotian Wang, Qianglong Chen, Weihua Peng, Xiaocheng Feng, Bing Qin, et al. A survey on hallucination in large language models: Principles, taxonomy, challenges, and open questions. *arXiv preprint arXiv:2311.05232*, 2023.

[57] K Mischaikow, T Kaczynski, and M Mrozek. Computational homology. *Applied Mathematical Sciences*, 157, 2004.

[58] Xiaojin Zhu. Persistent homology: An introduction and a new text representation for natural language processing. In *IJCAI*, pages 1953–1959, 2013.

[59] J Martin Bland and Douglas G Altman. Statistics notes: measurement error. *Bmj*, 312(7047):1654, 1996.

[60] Gaspard Monge. Mémoire sur la théorie des déblais et des remblais. *Mem. Math. Phys. Acad. Royale Sci.*, pages 666–704, 1781.

[61] Leonid V Kantorovich. On the translocation of masses. *Journal of mathematical sciences*, 133(4), 2006.

[62] Marco Cuturi. Sinkhorn distances: Lightspeed computation of optimal transport. *NeurIPS*, 26, 2013.

[63] Kevin Clark, Urvashi Khandelwal, Omer Levy, and Christopher D Manning. What does bert look at? an analysis of bert’s attention. *arXiv preprint arXiv:1906.04341*, 2019.

[64] Muhammad Uzair Khattak, Hanoona Rasheed, Muhammad Maaz, Salman Khan, and Fahad Shahbaz Khan. Maple: Multi-modal prompt learning. In *CVPR*, pages 19113–19122, 2023.

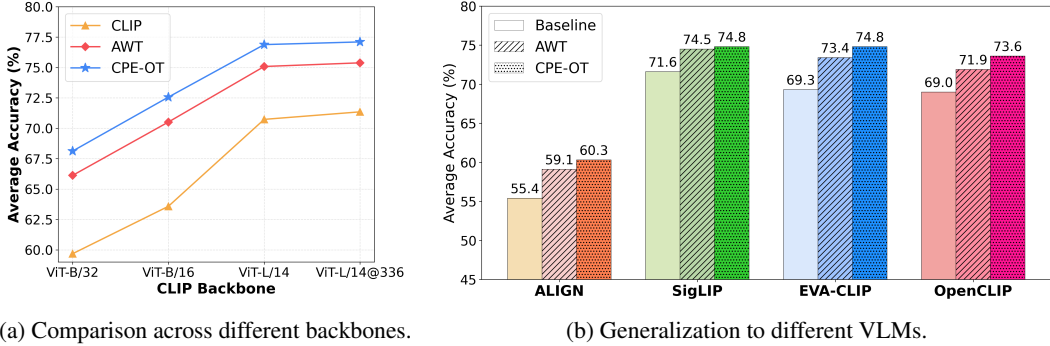
[65] Guangyi Chen, Weiran Yao, Xiangchen Song, Xinyue Li, Yongming Rao, and Kun Zhang. Plot: Prompt learning with optimal transport for vision-language models. In *ICLR*, 2022.

[66] Shuhuai Ren, Aston Zhang, Yi Zhu, Shuai Zhang, Shuai Zheng, Mu Li, Alexander J Smola, and Xu Sun. Prompt pre-training with twenty-thousand classes for open-vocabulary visual recognition. *NeurIPS*, 36: 12569–12588, 2023.

- [67] Chen Xu, Yuhang Zhu, Haocheng Shen, Boheng Chen, Yixuan Liao, Xiaoxin Chen, and Limin Wang. Progressive visual prompt learning with contrastive feature re-formation. *IJCV*, 133(2):511–526, 2025.
- [68] Vishaal Udandarao, Ankush Gupta, and Samuel Albanie. Sus-x: Training-free name-only transfer of vision-language models. In *ICCV*, pages 2725–2736, 2023.
- [69] Bolin Ni, Houwen Peng, Minghao Chen, Songyang Zhang, Gaofeng Meng, Jianlong Fu, Shiming Xiang, and Haibin Ling. Expanding language-image pretrained models for general video recognition. In *ECCV*, pages 1–18, 2022.
- [70] Taojiannan Yang, Yi Zhu, Yusheng Xie, Aston Zhang, Chen Chen, and Mu Li. Aim: Adapting image models for efficient video action recognition. In *ICLR*, 2022.
- [71] Junting Pan, Ziyi Lin, Xiatian Zhu, Jing Shao, and Hongsheng Li. St-adapter: Parameter-efficient image-to-video transfer learning. *NeurIPS*, 35:26462–26477, 2022.
- [72] Syed Talal Wasim, Muzammal Naseer, Salman Khan, Fahad Shahbaz Khan, and Mubarak Shah. Vita-clip: Video and text adaptive clip via multimodal prompting. In *CVPR*, pages 23034–23044, 2023.
- [73] Hanoona Rasheed, Muhammad Uzair Khattak, Muhammad Maaz, Salman Khan, and Fahad Shahbaz Khan. Fine-tuned clip models are efficient video learners. In *CVPR*, pages 6545–6554, 2023.
- [74] Shoufa Chen, Chongjian Ge, Zhan Tong, Jiangliu Wang, Yibing Song, Jue Wang, and Ping Luo. Adapt-former: Adapting vision transformers for scalable visual recognition. *NeurIPS*, 35:16664–16678, 2022.
- [75] Mehdi Cherti, Romain Beaumont, Ross Wightman, Mitchell Wortsman, Gabriel Ilharco, Cade Gordon, Christoph Schuhmann, Ludwig Schmidt, and Jenia Jitsev. Reproducible scaling laws for contrastive language-image learning. In *CVPR*, pages 2818–2829, 2023.

## A Generalization across Various Architectures

We conduct evaluations across various CLIP architectures, exploring the model’s scalability from ViT-B/32 to ViT-L/14@336. As shown in Figure 4a, our CPE-OT consistently outperforms AWT by approximately 2%. Additionally, we assess the model’s generalization on four other VLMs: ALIGN [4], SigLIP [36], EVA-CLIP [37], and OpenCLIP [75], with results shown in Figure 4b. AWT achieves a 3% improvement over the baseline, while our CPE-OT provides an additional 1% boost over AWT. These results demonstrate that our method consistently achieves performance improvements across all evaluated scenarios, highlighting its generalization.



(a) Comparison across different backbones.

(b) Generalization to different VLMs.

Figure 4: **Generalizing across architectures.** Average top-1 accuracy (%) on 10 zero-shot image datasets is reported.

## B Efficiency Analysis

In Table 6, we compare the token consumption for text generation and the inference time during testing. Compared to the current competitive two-step dataset-aware prompting strategy (rows 5 and 6), our method requires only an additional 1% of tokens to generate synonyms, while achieving a more than 2% improvement in zero-shot recognition performance. At the same time, our method increases inference time by only 0.5% compared to AWT. These results demonstrate that our approach significantly enhances zero-shot task performance while maintaining high inference efficiency and computational resource utilization.

Model	LLMs Generator Requirements		Token Usage	Inference Time (s)	Accuracy (%)
	Words (10K)	Sentences (500K)			
CLIP [1]	-	-	-	0.035	63.58
CuPL [47]	-	1	500K	0.035	65.15
REAL [14]	1	-	10K	0.035	66.33
TPS [12]	-	-	-	0.186	66.95
MPVR [50]	-	2	1000K	0.035	69.61
AWT [13]	-	2	1000K	0.103	70.51
CPE-OT	1	2	1010K	0.108	<b>72.56</b>

Table 6: Efficiency analysis across different methods. For every 1K categories, LLMs generate approximately 10K tokens for words and 500K tokens for sentences (refer to [14]). Inference Time reports the average inference time per image (in seconds).

## C Pipeline of Set-to-set Visual-textual Matching

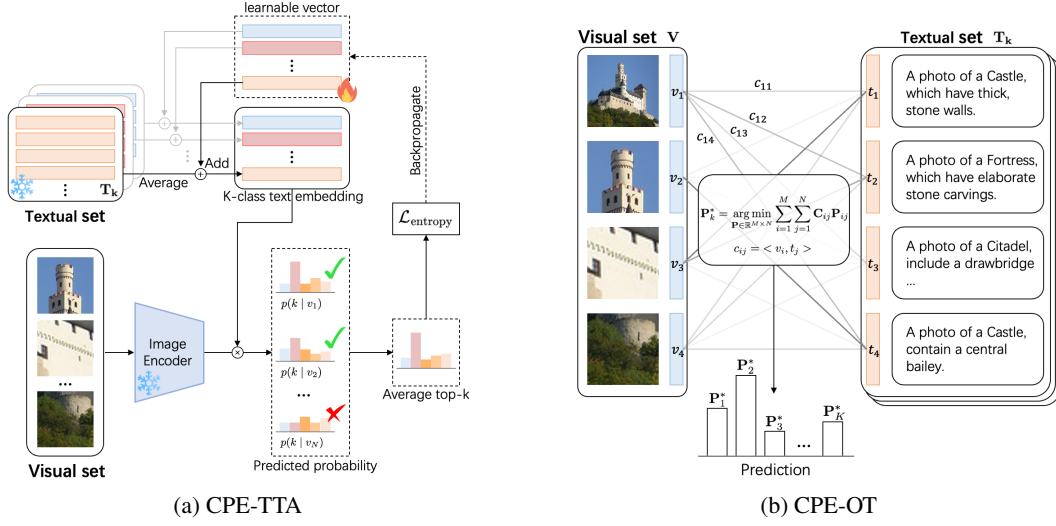


Figure 5: Pipeline of CPE-TTA and CPE-OT.

## D Additional Details

### D.1 Error bar analysis

We conducted an analysis of error bars across 15 image datasets, each evaluated with three different random seeds to ensure statistical robustness. The results, presented in Table 7, show that our method consistently achieves robust performance with minimal variability on most datasets.

Method	Oxford Flowers	DTD	Oxford Pets	Stanford Cars	UCF101
CLIP	67.44	44.27	88.25	65.48	65.13
CPE-OT	84.14±0.13	57.84±0.07	92.44±0.13	69.99±0.16	73.05±0.01
Method	Caltech101	Food101	SUN397	FGVC Aircraft	EuroSAT
CLIP	93.35	83.65	62.59	23.67	42.01
CPE-OT	95.67±0.10	86.04±0.04	70.56±0.09	32.64±0.05	62.96±0.64
Method	ImageNet-1k	ImageNet-A	ImageNet-V2	ImageNet-R	ImageNet-K
CLIP	66.74	47.74	60.75	73.98	46.13
CPE-OT	71.70±0.04	60.09±0.03	65.47±0.02	80.46±0.22	52.78±0.06

Table 7: Error bar analysis on 15 image datasets. The mean and the standard deviation of the top-1 accuracy is reported.

### D.2 License information

**Datasets.** Below are the datasets used in this paper that have known license information: (1) MIT License: ImageNet-A [30], ImageNet-V2 [31], ImageNet-R [32], ImageNet-Sketch [33], EuroSAT [28]. (2) CC BY 4.0 License: HMDB51 [34], Kinetics-600 [35]. (3) CC BY-SA 4.0 License: Oxford Pets [21].

**Source code.** Source code used in this paper are under the MIT License: CLIP [1], CoOp [39], TPT [51], PLOT [65], REAL [14].

## E Limitations

Despite the promising results, our method has several limitations. First, the generation of synonyms relies heavily on the quality of LLM outputs, which may produce inconsistent results across different LLM versions or prompting strategies. Second, our activation map-based approach for discriminative region selection may struggle with images containing complex scenes where foreground-background separation is ambiguous. Third, the improvement in performance comes with a slight increase in computational overhead during inference, which may affect real-time applications.